

# Semiconducting electrides derived from Sodalite: A first-principles study

Chang Liu,<sup>1</sup> Mahfuza Mukta,<sup>2</sup> Byungkyun Kang,<sup>3,\*</sup> and Qiang Zhu<sup>2,†</sup>

<sup>1</sup>*Department of Physics and Astronomy, University of Nevada, Las Vegas, NV 89154, USA*

<sup>2</sup>*Department of Mechanical Engineering and Engineering Science,*

*University of North Carolina at Charlotte, Charlotte, NC 28223, USA*

<sup>3</sup>*College of Arts and Sciences, University of Delaware, Newark, Delaware 19716, USA*

(Dated: September 27, 2024)

Electrides are ionic crystals with electrons acting as anions occupying well-defined lattice sites. These exotic materials have attracted considerable attention in recent years for potential applications in catalysis, rechargeable batteries, and display technology. Among this class of materials, electride semiconductors can further expand the horizon of potential applications due to the presence of a band gap. However, there are only limited reports on semiconducting electrides, hindering the understanding of their physical and chemical properties. In a recent work, we initiated an approach to derive potential electrides via selective removal of symmetric Wyckoff sites of anions from existing complex minerals. Herein, we present a follow-up effort to design the semiconducting electrides from parental complex sodalites. Among four candidate compounds, we found that a cubic  $\text{Ca}_4\text{Al}_6\text{O}_{12}$  structure with the  $I-43m$  space group symmetry exhibits perfect electron localization at the sodalite cages, with a narrow electronic band gap of 1.2 eV, making it suitable for use in photocatalysis. Analysis of the electronic structures reveals that a lower electronegativity of surrounding cations drives greater electron localization and promotes the formation of an electride band near the Fermi level. Our work proposes an alternative approach for designing new semiconducting electrides under ambient conditions and offers guidelines for further experimental exploration.

## I. INTRODUCTION

Electrides are exotic ionic materials in which electrons occupy the well-defined lattice sites and serve the role of anions. These materials were originally discovered by Dye and coworkers in organic salts in the 1980s, however, their high sensitivity to heat and oxidation limits their practical application<sup>1,2</sup>. Subsequent efforts have been directed towards achieving stable electrides, aiming to explore chemical and physical properties arising from nearly-free electrons and their corresponding geometric topologies. In 2003, the first thermally stable electride  $\text{Ca}_6\text{Al}_7\text{O}_{16}$  ( $\text{C12A7:2e}^-$ ) was synthesized from the inorganic mineral mayenite ( $12\text{CaO}\cdot 7\text{Al}_2\text{O}_3$ )<sup>3</sup>. The resulting electride, with excess electrons confined in zero dimensional (0D) cages, exhibits excellent thermal stability and low reactivity with air. This discovery marks a milestone in the research on electrides, and spurred numerous new efforts to design other novel inorganic electrides. To date, electrides have been identified in various inorganic compounds exhibiting different configurations of confined electrons<sup>4,5</sup>, including 0D cavities<sup>3,6,7</sup>, 1D chains<sup>8–12</sup>, 2D planes<sup>13–17</sup>, and 3D configurations<sup>18</sup>. These diverse electronic configurations produce unique properties, including high electron concentration<sup>13,19</sup>, anti-ferromagnetism<sup>11</sup>, thermionic electron emission at low temperature<sup>13,20</sup>, high density of active sites<sup>21</sup>, and low work function<sup>22</sup>. These exceptional properties make electrides promising candidates for applications in catalysis<sup>23,24</sup>, energy storage<sup>25,26</sup>, and electronics<sup>27,28</sup>.

While most currently reported electrides are semi-metals, an electride with semiconducting band structure has the potential to further expand the horizon of potential applications of such electrides as infrared photodetector<sup>29</sup>. Previous theoretical study proposed a transition in  $\text{Ca}_2\text{N}$  from 2D conducting electride to a 0D semiconducting electride state under high pressure<sup>30</sup>. This discovery was supported by electrical resis-

tance measurements conducted in a follow-up experimental study<sup>31</sup>. To further investigate physical and chemical properties and explore possible applications of semiconducting electrides, stable structures at ambient conditions still need to be developed<sup>32</sup>. In 2022, a novel inorganic electride,  $\text{Sc}_2\text{C}$ , was discovered as the first 2D electride exhibiting semiconducting behavior<sup>29</sup>. Its small band gap and good conductivity enable applications as a battery electrode or in IR photodetectors. Recent theoretical study identified  $\text{Mg}_2\text{N}$  in  $R3m$  symmetry as a 0D electride with a semiconducting band structure<sup>33</sup>. But research on this novel class of electrides is still in its infancy. Consequently, discovering new semiconducting electrides with different confined electron configurations stabilized at ambient conditions is essential to understand related properties and new electride design towards potential applications.

Recently, we introduced an alternative method to achieve electride states by removing high-symmetry Wyckoff sites of anions from existing sodalite compounds<sup>34</sup>. The resulting sodalite electrides are expected to exhibit greater thermal stability due to their intricate structural framework, thereby holding promise for practical applications. In our previous work, we primarily focused on halides, where only one electron can be accommodated per cage in the resulting sodalite framework (see Fig. 1). Consequently, the localized cage electrons can lead to either a half-metallic state or a Mott insulator from the perspective of electron counts<sup>34</sup>. According to the electron counting rule, it is likely that two localized electrons in a cage of the crystal structure may form a distinct electronic band with full occupation, leading to a semiconducting or insulating band structure. Although this simple model may be complicated by the interplay between the cage electrons and their surrounding cations, we hypothesize that this is a viable approach to design new electride materials with a nonzero band gap. Therefore, we have decided to further explore this av-

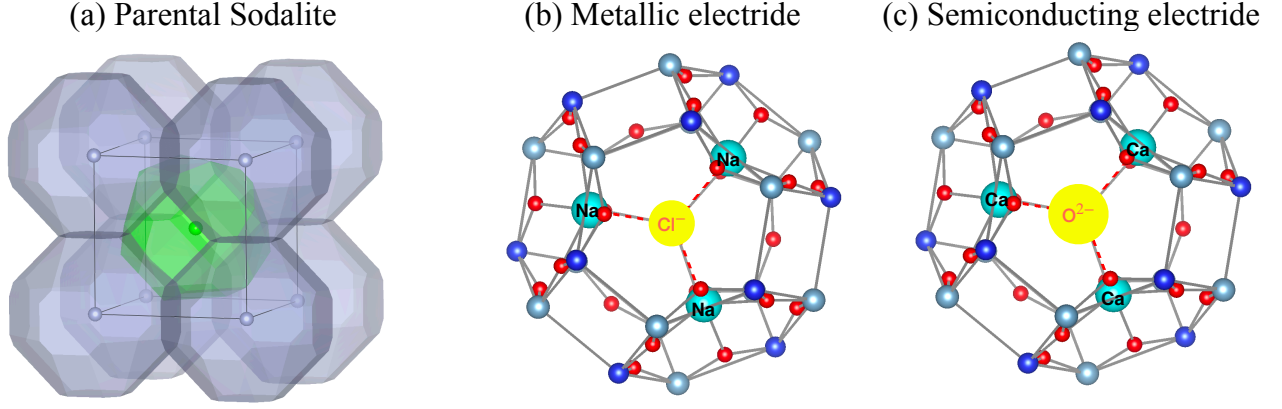


FIG. 1. The schematic illustration of electride properties

enue by investigating sodalite compounds that contain high-symmetry Wyckoff sites of anions with a -2 formal charge.

In this work, we applied a screening strategy similar to our previous study<sup>34</sup> on existing multi-component sodalites and identified four candidate parental structures characterized by the presence of chalcogen anions in high-symmetry Wyckoff sites. These candidates include  $\text{Ca}_4\text{Al}_6\text{O}_{13}$ ,  $\text{Zn}_4\text{B}_6\text{O}_{13}$ ,  $\text{Cd}_4\text{Al}_6\text{SO}_{12}$ , and  $\text{Be}_3\text{Cd}_4\text{Si}_3\text{SeO}_{12}$ . We initially examined the lattice dynamical properties of these structures after removing the anionic site at the center of the unit cell. Theoretical results indicate that the generated compounds are dynamically stable under ambient conditions. Subsequently, we conducted electronic structure calculations on these derivative compounds to verify the presence of electride states. Interestingly, we found that these sodalite compounds, with various metal cations adjacent to the electride site, provide an ideal platform for exploring systematic trends. Our further analysis of the evolution of electronic properties with the adjacent cations revealed that a lower electronegativity of the adjacent cation can stabilize the electride states and generate a distinct electride band around the Fermi level.

## II. COMPUTATIONAL METHODS

Following a query of the Materials Project<sup>35</sup> using our in-house symmetry analysis toolbox, `PyXtal`<sup>36</sup>, we selected four complex sodalite structures in cubic symmetry,  $\text{Ca}_4\text{Al}_6\text{O}_{13}$ ,  $\text{Zn}_4\text{B}_6\text{O}_{13}$ ,  $\text{Cd}_4\text{Al}_6\text{SO}_{12}$ , in  $I-43m$  space group and  $\text{Cd}_4\text{Be}_3\text{Si}_3\text{SeO}_{12}$  in  $P43n$  space group as parent structures to create the electride phases. For each structure, the electride configuration was generated by removing the anions at the center of the unit cell. The structures were then fully relaxed to obtain optimal cell parameters, and their structural stability was checked using phonon calculations. All calculations were performed using the projector augmented wave (PAW) method<sup>37</sup>, implemented in the `VASP` code<sup>38</sup> within the framework of density functional theory (DFT). The generalized gradient approximation (GGA) with the Perdew, Burke, and Ernzerhof (PBE) functional<sup>39</sup> was adopted. For geometric relaxation, we used a unit cell containing two formula units

and a  $3 \times 3 \times 3$   $\Gamma$ -centered k-point grid was adopted. To simulate electronic properties, a primitive cell with a dense mesh of  $8 \times 8 \times 8$  k-point grid was utilized. The cutoff energy for all calculations was set to 520 eV, achieving convergence for energy around 1 meV per atom and for forces within 0.01 eV/Å. For phonon calculations, the optimized structures for electrides were used to construct a  $2 \times 2 \times 2$  supercell (containing 176 atoms), employing a single  $\Gamma$  point for Brillouin zone sampling. Phonon density of states were calculated using force constants obtained via the finite displacement method implemented in the `Phonopy` code<sup>40</sup>.

## III. RESULTS AND DISCUSSIONS

### A. Crystal Structures

In this work, all four candidate parental oxides have already been observed in experiment<sup>41–44</sup>. As shown in Fig. 2, each unit cell contains two formula units. According to X-ray diffraction analysis<sup>41</sup>,  $\text{Ca}^{2+}$  is bonded to four  $\text{O}^{2-}$  atoms to form distorted  $\text{CaO}_4$  trigonal pyramids that share corners with six equivalent  $\text{AlO}_4$  tetrahedra and corners with three equivalent  $\text{CaO}_4$  trigonal pyramids. Other materials, including  $\text{Zn}_4\text{B}_6\text{O}_{13}$ ,  $\text{Cd}_4\text{Al}_6\text{SO}_{12}$ , and  $\text{Cd}_4\text{Be}_3\text{Si}_3\text{SeO}_{12}$  show the similar packing behavior. Table I summarizes the calculated cell parameters, which align well with experimental data, thus confirming the choice of DFT calculation parameters.

For each structure, we removed the cage anions at the body center of the unit cells to generate candidate electride structures. Specifically, we removed  $\text{O}^{2-}$  for  $\text{Ca}_4\text{Al}_6\text{O}_{13}$  and  $\text{Zn}_4\text{B}_6\text{O}_{13}$ ,  $\text{S}^{2-}$  for  $\text{Cd}_4\text{Al}_6\text{SO}_{12}$ , and  $\text{Se}^{2-}$  for  $\text{Cd}_4\text{Be}_3\text{SeO}_{12}$ . Correspondingly, the resulting candidate electride structures consist cages surrounded by four  $\text{Ca}^{2+}$  in  $\text{Ca}_4\text{Al}_6\text{O}_{12}$ , four  $\text{Zn}^{2+}$  in  $\text{Zn}_4\text{B}_6\text{O}_{12}$ , four  $\text{Cd}^{2+}$  in both  $\text{Cd}_4\text{Al}_6\text{O}_{12}$  and  $\text{Cd}_4\text{Be}_3\text{Si}_3\text{O}_{12}$ . Comparing the cell parameters between the parental and anion-removal phases, we found that most of the systems undergo a lattice shrink after the removal of anions (see Table I). However, the  $\text{Ca}_4\text{Al}_6\text{O}_{12}$  is an exception. After the removal of  $\text{O}^{2-}$ , the volume unexpectedly increases, suggesting that new types of interactions may

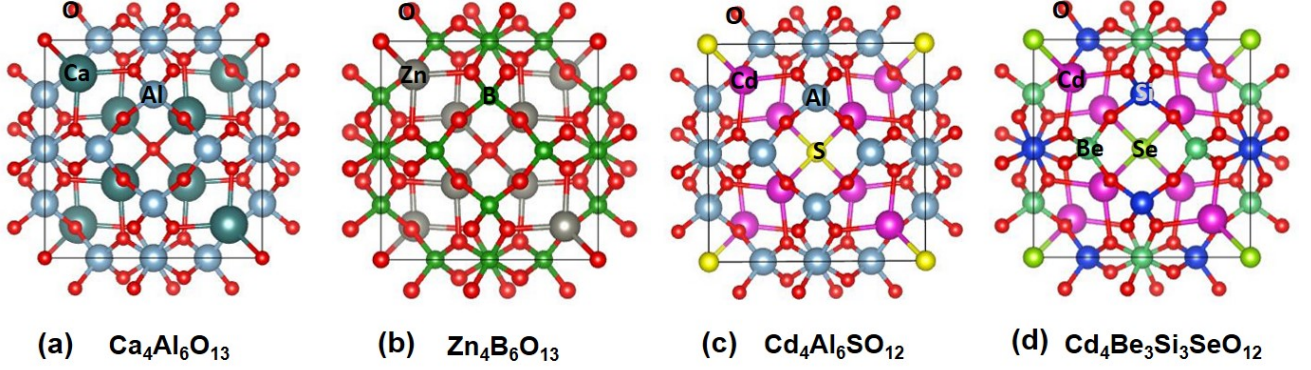


FIG. 2. Crystal structures of (a)  $\text{Ca}_4\text{Al}_6\text{O}_{13}$ , (b)  $\text{Zn}_4\text{B}_6\text{O}_{13}$ , (c)  $\text{Cd}_4\text{Al}_6\text{SO}_{12}$ , (d)  $\text{Cd}_4\text{Be}_3\text{Si}_3\text{SeO}_{12}$ . The high symmetry cage anion sites are located at the body center position in each structure.

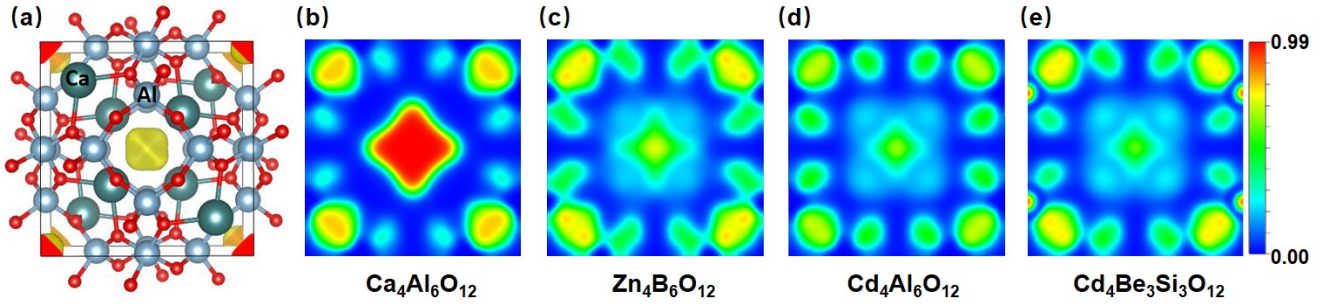


FIG. 3. Calculated electron localization function (ELF) after the removal of  $\text{O}^{2-}$ . (a) the 3D ELF isosurface ELF of  $\text{Ca}_4\text{Al}_6\text{O}_{12}$ . (b-e) 2D ELF of  $\text{Ca}_4\text{Al}_6\text{O}_{12}$ ,  $\text{Zn}_4\text{B}_6\text{O}_{12}$ ,  $\text{Cd}_4\text{Al}_6\text{O}_{12}$ ,  $\text{Cd}_4\text{Be}_3\text{Si}_3\text{O}_{12}$  in the (200) plane.

TABLE I. The crystallographic data and band gaps of four parent sodalites and their derivative electrode candidate structures.

| System   | Space Group    | $a$ (Å) |             | Band Gap (eV) |
|--|----------------|---------|-------------|---------------|
|  |                | DFT     | Expt.       |               |
| Sodalites  |                |         |             |               |
| $\text{Ca}_4\text{Al}_6\text{O}_{13}$              | $I\text{-}43m$ | 8.87    | $8.86^{41}$ | 3.9           |
| $\text{Zn}_4\text{B}_6\text{O}_{13}$               | $I\text{-}43m$ | 7.55    | $7.47^{42}$ | 3.4           |
| $\text{Cd}_4\text{Al}_6\text{SO}_{12}$             | $I\text{-}43m$ | 8.95    | $8.82^{43}$ | 2.7           |
| $\text{Cd}_4\text{Be}_3\text{Si}_3\text{SeO}_{12}$ | $P43n$         | 8.62    | $8.49^{44}$ | 2.9           |
| Electride candidates                               |                |         |             |               |
| $\text{Ca}_4\text{Al}_6\text{O}_{12}$              | $I\text{-}43m$ | 9.06    |             | 1.2           |
| $\text{Zn}_4\text{B}_6\text{O}_{12}$               | $I\text{-}43m$ | 7.41    |             | 3.6           |
| $\text{Cd}_4\text{Al}_6\text{O}_{12}$              | $I\text{-}43m$ | 8.64    |             | 2.7           |
| $\text{Cd}_4\text{Be}_3\text{Si}_3\text{O}_{12}$   | $P43n$         | 8.22    |             | 3.0           |

form due to the localized cage electrons.

Additionally, we computed the phonon spectrum for each structure and found that none exhibit imaginary frequencies (see Fig. S1 in the supplementary materials). This indicates that all structures remain dynamically stable after the removal of cage anions, allowing them to persist as long as they are synthesized in experimental conditions.

## B. Spatial Electron Localization

To characterize the electrides state, we calculated the electron localization function (ELF), which measures the degree of electron's spatial localization compared to a reference electron with the same spin. The ELF value, bounded between 0 and 1, reflects the likelihood of finding an electron in the neighborhood of a reference electron located at a given point in which  $\text{ELF} = 1$  corresponding to perfect localization and  $\text{ELF} = 0.5$  corresponding to free electron gas<sup>45</sup>.

As shown in Fig. 3, we observed strong ELF values at the body center cages after the removal of the cage anions from the parent structures. These results suggest that the electrons remain localized at the sodalite cages. Among them,  $\text{Ca}_4\text{Al}_6\text{O}_{12}$  possesses an ELF value of 0.99 at the body center, suggesting the strongest electron localization. On the other hands, the ELF values at the cage centers for  $\text{Zn}_4\text{B}_6\text{O}_{12}$ ,  $\text{Cd}_4\text{Al}_6\text{O}_{12}$  and  $\text{Cd}_4\text{Be}_3\text{Si}_3\text{O}_{12}$  are 0.72, 0.65 and 0.59, respectively. The trend of the ELF values has strong correlation with the electronegativity of the surrounding metal cations. Ca has an electronegativity value of 1.00, whereas Zn has a value of 1.65 and Cd of 1.69<sup>46</sup>. Due to its lower electronegativity compared to  $\text{Zn}^{2+}$  and  $\text{Cd}^{2+}$  cations,  $\text{Ca}^{2+}$  is expected to have a weaker attraction to the outer core electrons, consequently leading to the greater electron localization at the body center cages in  $\text{Ca}_4\text{Al}_6\text{O}_{12}$ .



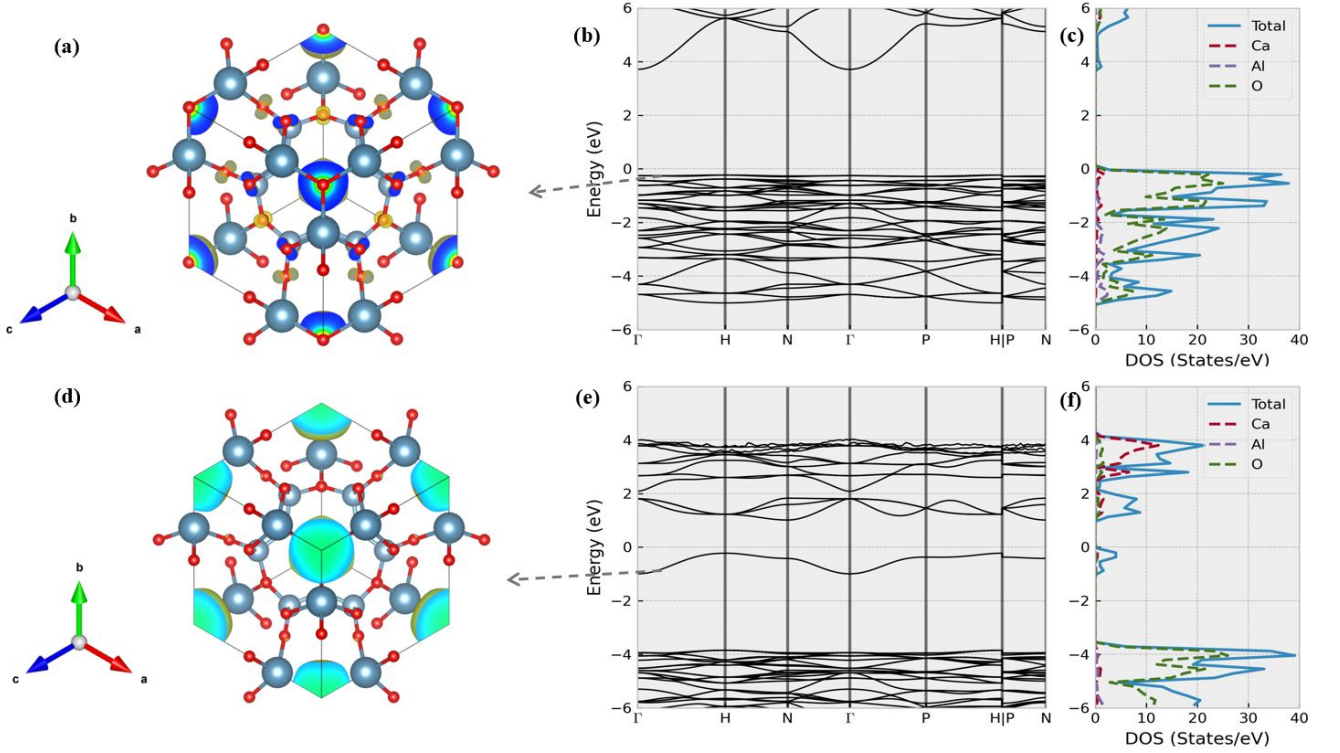


FIG. 4. Electronic structures of  $\text{Ca}_4\text{Al}_6\text{O}_{13}$  and  $\text{Ca}_4\text{Al}_6\text{O}_{12}$ . (a) displays the isosurface of the decomposed charge density of  $\text{Ca}_4\text{Al}_6\text{O}_{13}$ 's highest valence band, whereas (b) and (c) plot its band dispersion and density of states (DOS) at an extended energy range around the Fermi level. As a comparison, (d)-(f) show the isosurface of the decomposed charge density of  $\text{Ca}_4\text{Al}_6\text{O}_{12}$ 's highest conduction band and its corresponding band structure and DOS plots. The isosurface value is set as  $0.003 \text{ e/bohr}^3$  in (a) and (d).

### C. Electronic Band Structures

In addition to the electron's spatial localization, we are also interested in understanding their electronic band structures and the energy levels of those localized cage electrons. As shown in Fig. 4b, the parent structure  $\text{Ca}_4\text{Al}_6\text{O}_{13}$  is a semiconductor with a band gap of 3.9 eV, and the highest valence band (HVB) near the Fermi level are very flat. The associated DOS plot (Fig. 4c) suggests that HVB is mainly contributed by the O orbitals, while the conduction bands comprise the hybridization of oxygen and metal atoms. More precisely, we can clearly see that the decomposed charge density of HVB is mainly featured by the electrons around the  $\text{O}^{2-}$  anions at the cage center, as shown in Fig. 4a. Overall, the HVB in  $\text{Ca}_4\text{Al}_6\text{O}_{13}$  has an energy close to other valance bands.

After the removal of cage  $\text{O}^{2-}$  anions, the resulting structure maintains a semiconducting band structure with a much narrower band gap of 1.2 eV. As shown in both Fig. 3d and e, the  $\text{Ca}_4\text{Al}_6\text{O}_{12}$  has a HVB clearly separated from other valence bands in the systems. Remarkably, the computed partial charge configuration in Fig. 4d, unlike what is shown in Fig. 4a, suggests that this band solely correspond to electrons localized at cage centers.

This scenario can be simply understood from the electron counting rule as we presented earlier. When O is present at the cage center, each O has the capability to attract excess elec-

trons to from four neighboring Ca atoms, leading to a charge transfer from Ca to O and forming the ionic bonding between  $\text{O}^{2-}$  and  $\text{Ca}^{2+}$ . This ionic bonding can also helps to lower the valence band energy. When the cage O atoms are removed, the excess electrons from the Ca atoms cannot be redistributed to any surrounding cations. As a result, the localized cage electrons behaves like a nucleus-free anions to stabilize the crystal structure. If there is only one electron in each cage, the system should form a partially occupied band as discussed in our previous work<sup>34</sup>. Given that two electrons are present in each cage of  $\text{Ca}_4\text{Al}_6\text{O}_{12}$ , these electrons forms a fully occupied electronic band. And the whole structure remains semiconducting. However, this band is expected to possess a higher energy as compared to the counterpart HVB in  $\text{Ca}_4\text{Al}_6\text{O}_{13}$ . Notably, the repulsion between localized cage electrons and surrounding  $\text{Ca}^{2+}$  in  $\text{Ca}_4\text{Al}_6\text{O}_{12}$  also tend to expand the  $[\text{Ca}]_4$  tetrahedra and thus leads a larger volume as compared to the parental phase. Therefore, the band gap in  $\text{Ca}_4\text{Al}_6\text{O}_{12}$  becomes smaller. And we can safely conclude that  $\text{Ca}_4\text{Al}_6\text{O}_{12}$  is a typical electride feature with a semiconducting band gap. To our knowledge, this is the first report of non-layered electride phase that can be stabilized at ambient pressure conditions.

While the case of  $\text{Ca}_4\text{Al}_6\text{O}_{12}$  demonstrate the possibility to achieve a energy band fully occupied by interstitial electrons near the Fermi level, the interplay with the local chemical environment may complicate this scenario. As shown in Fig. 5, the parent system  $\text{Cd}_4\text{Al}_6\text{SO}_{12}$  is a semiconductor with a band

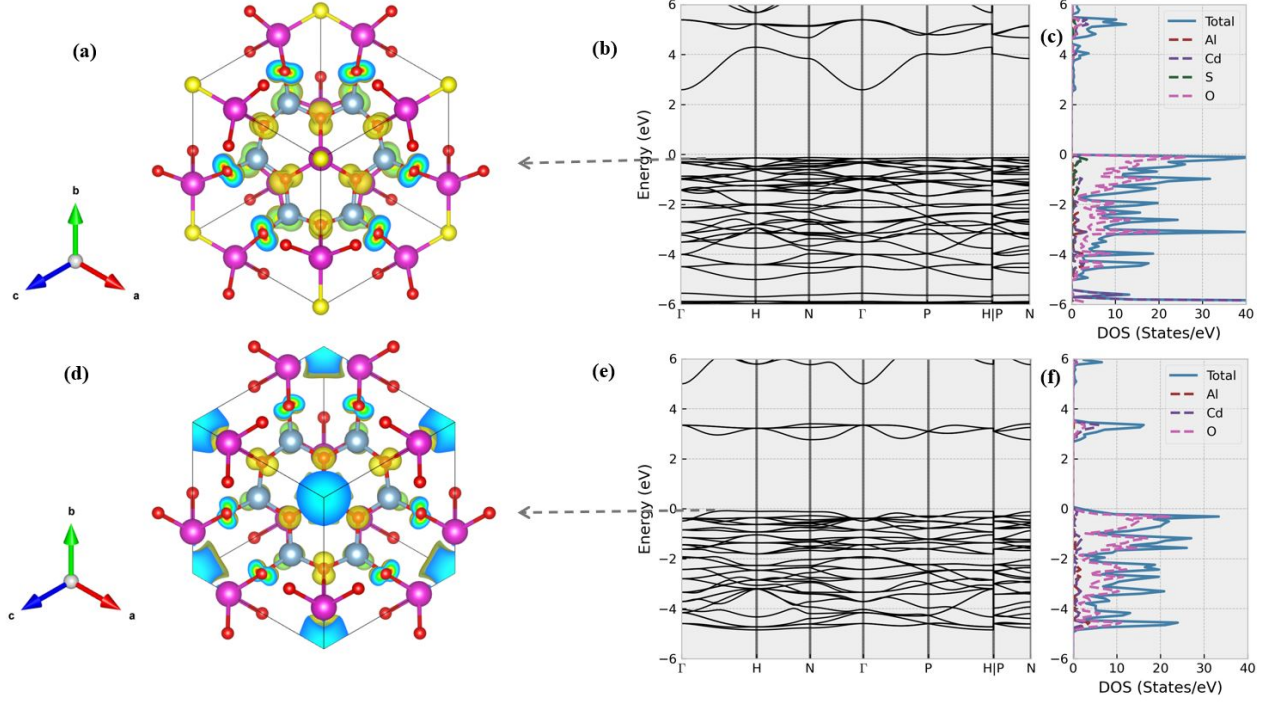


FIG. 5. Electronic structures of the  $\text{Cd}_4\text{Al}_6\text{SO}_{12}$  and  $\text{Cd}_4\text{Al}_6\text{O}_{12}$ . (a) displays the decomposed charge density of  $\text{Cd}_4\text{Al}_6\text{SO}_{12}$ 's highest valence band, whereas (b) and (c) plot its band dispersion and DOS at the extended range. As a comparison, (d)-(f) show the isosurface of the decomposed charge density of  $\text{Cd}_4\text{Al}_6\text{O}_{12}$ 's highest valence band, as well as its corresponding band structure and DOS plots. The isosurface value is set as  $0.003 \text{ e/bohr}^3$  in (a) and (d).

gap of 2.7 eV. The top valence bands near the Fermi level of  $\text{Cd}_4\text{Al}_6\text{SO}_{12}$  mainly come from O, S and Cd atoms. Upon removing the S atoms, we can find several high energy conduction bands drop off, similar to those in  $\text{Ca}_4\text{Al}_6\text{O}_{12}$ . However, the band gap of the  $\text{Cd}_4\text{Al}_6\text{O}_{12}$  does not vary significantly from that of the parent structure. This is also evidenced by the visualization of partial charge density of the valence band closest to the Fermi level (see Fig. 5d). While there exist localized electrons around the cage center, we also find a significant portion of electrons around the neighboring O atoms (that are similar to the parental compound). Therefore, we can better interpret this band reflects an interaction between  $\text{Cd}_4$  cluster cations and neighboring O anions. Compared to cage electrons in  $\text{Ca}_4\text{Al}_6\text{O}_{12}$ , the cage electrons in  $\text{Cd}_4\text{Al}_6\text{O}_{12}$  are tightly bounded by the Cd nucleus. Therefore the charge redistribution after the removal of S atoms in  $\text{Cd}_4\text{Al}_6\text{SO}_{13}$  fails to generate an isolated energy band fully occupied by interstitial electrons near the Fermi level. We also observed a similar trend in  $\text{Cd}_4\text{Be}_3\text{Si}_3\text{SeO}_{12}$  (see Fig. S2 in the supplementary materials). In this system, the corresponding partial charge density plot in  $\text{Cd}_4\text{Be}_3\text{Si}_3\text{O}_{12}$  reveals that O contribute more portions as compared to the cage electrons, suggesting that the substitution of Be and Si can systematically shift the charge redistribution.

As shown in Fig. 6,  $\text{Zn}_4\text{B}_6\text{O}_{13}$  is a semiconductor with a band gap of 3.9 eV. Its valence bands near the Fermi level are contributed by Zn and non-cage O atoms. Following the removal of cage O atoms, we observe a lowering of several high-

energy conduction bands, similar to what is found in other systems. According to Fig. 6f, these bands correspond to the anti-bonding states with localized electrons around the cage. However, we do not find significant electron density around the cage in the top valence bands. Instead, the HVB of  $\text{Zn}_4\text{B}_6\text{O}_{13}$  in  $\text{Zn}_4\text{B}_6\text{O}_{12}$  mainly consist of electrons around non-cage O and Zn atoms (see Fig. 6e). This suggests that the majority of excess electrons tend to return to the Zn atoms rather than remaining localized around the cage. Consequently, the band gap of  $\text{Zn}_4\text{B}_6\text{O}_{12}$  does not vary significantly from that of the parent structure.

Finally, we present the partial charge distribution in the top valence bands of  $\text{Ca}_4\text{Al}_6\text{O}_{12}$ ,  $\text{Cd}_4\text{Al}_6\text{O}_{12}$ ,  $\text{Zn}_4\text{B}_6\text{O}_{12}$  in Fig. 7, where atomic spheres in the unit cell have been removed for clarity. These plots illustrate how the two excess electrons are redistributed following the removal of the cage atoms. In  $\text{Ca}_4\text{Al}_6\text{O}_{12}$ , the high valence band (HVB) charge density indicates that the excess electrons remain localized within the cage. However, this arrangement is energetically unfavorable, leading to an upward shift of the HVB in its band structure and a consequent reduction of the band gap. Upon replacing Ca with Cd, the electronic behavior in  $\text{Cd}_4\text{Al}_6\text{O}_{12}$  changes significantly. Due to Cd's higher electronegativity, a portion of the cage electrons is redistributed towards the Cd nucleus, as shown in Fig. 7b. In  $\text{Zn}_4\text{B}_6\text{O}_{12}$ , the charge redistribution is even more pronounced (see Fig. 7c). Here, the majority of excess electrons accumulate around the Zn nucleus due to the attractive forces from both neighboring Zn and B nuclei.

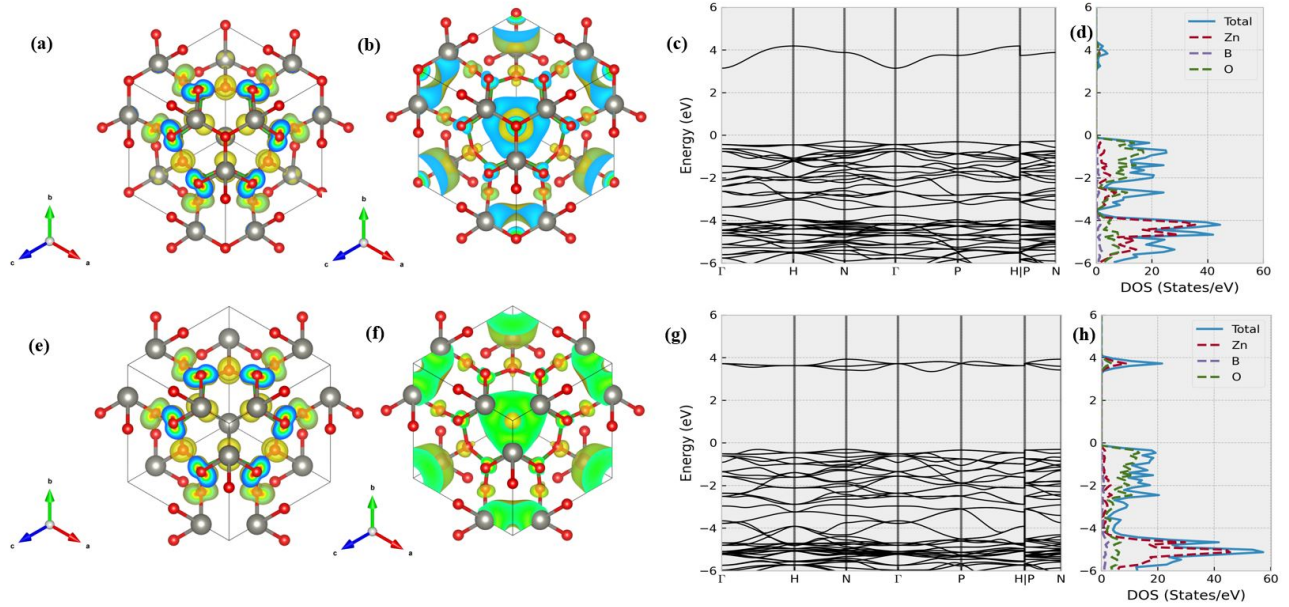


FIG. 6. Electronic structures of the  $\text{Zn}_4\text{B}_6\text{O}_{13}$  and  $\text{Zn}_4\text{B}_6\text{O}_{12}$ . (a) and (b) displays the decomposed charge densities of  $\text{Zn}_4\text{B}_6\text{O}_{13}$ 's highest valence band and lowest conduction band, whereas (c) and (d) plot its band dispersion and DOS at the extended range. As a comparison, (e)-(h) show the isosurface of the decomposed charge density of  $\text{Zn}_4\text{B}_6\text{O}_{12}$ 's highest valence band, lowest conduction band, the full band structure and DOS plots. The isosurface value is set as  $0.003 \text{ e/bohr}^3$  in (a), (b), (e) and (f).

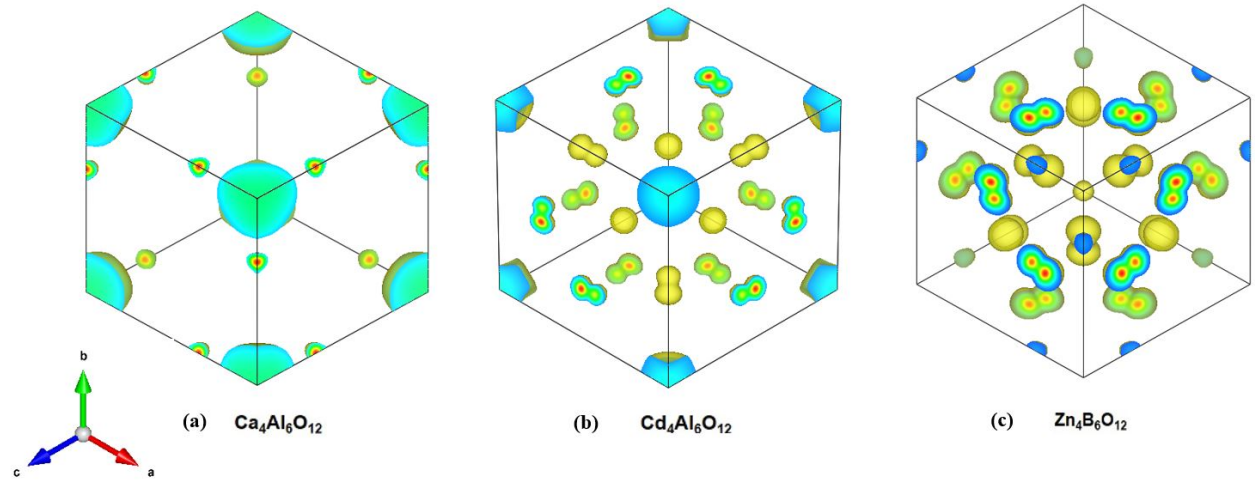


FIG. 7. The comparison of charge redistributions after the removal of cage atoms in the (a)  $\text{Ca}_4\text{Al}_6\text{O}_{12}$ , (b)  $\text{Cd}_4\text{Al}_6\text{O}_{12}$  and (c)  $\text{Zn}_4\text{B}_6\text{O}_{12}$ . In order to track the charge density near the atomic nucleus, the atomic spheres were intentionally omitted for clarity. The isosurface value is set as  $0.004 \text{ e/bohr}^3$  to remove some very small charge densities.

In both  $\text{Zn}_4\text{B}_6\text{O}_{12}$  and  $\text{Cd}_4\text{Al}_6\text{O}_{12}$ , this charge redistribution contributes to maintaining a low energy state, resulting in no significant band gap reduction in these systems.

From the above analysis, we find that after removing the cage center atoms in the sodalite structures, all systems may accommodate electrons at the cage center. However, these electrons may not be sufficient to generate a fully occupied energy band near the Fermi level. The electronegativity of the cations adjacent to the cage plays a crucial role in this

phenomenon. Among the four systems studied, only the cage electrons surrounded by the electron-rich  $\text{Ca}^{2+}$  cations form a fully occupied valence band near the Fermi level. These electrons create an anionic electronic sphere, which interacts weakly with the neighboring  $\text{Ca}^{2+}$  cations. In contrast, the cage electrons in the other systems may be redistributed to the neighboring  $\text{Cd}^{2+}$  or  $\text{Zn}^{2+}$  cations, preventing them from being considered as nucleus-free anions. This observation aligns with our previous screening work<sup>5</sup>, which indicated that only



group I, II, and early transition metals can form electrides.

#### IV. CONCLUSIONS

In this work, we conducted a survey to design new semiconducting electrides by selectively removing anions from existing sodalite structures. Our simulations reveal notable electron localization near the cage center after the removal of anions occupying the high-symmetry Wyckoff sites in the sodalite structures. However, the localized cage electrons may or may not form a distinct electride state in the electronic band structure, primarily depending on the electronegativity of the surrounding cations near the sodalite cages. Among the candidate compounds,  $\text{Ca}_4\text{Al}_6\text{O}_{12}$  serves as an ideal example of electron localization, capable of forming a fully occupied en-

ergy band near the Fermi level. This leads to a semiconducting electride with a significantly reduced band gap of 1.2 eV, compared to the parental sodalite structure's band gap of 3.9 eV. Additionally, this phase may exhibit improved thermal stability due to its complex structural framework. We hope that our findings will guide further experimental designs for new semiconducting electrides.

#### ACKNOWLEDGMENTS

This research was sponsored by the U.S. Department of Energy, Office of Science, Office of Basic Energy Sciences and the Established Program to Stimulate Competitive Research (EPSCoR) under the DOE Early Career Award No. DE-SC0021970. The computing resources are provided by ACCESS (TG-DMR180040).

- 
- \* [bkang@udel.edu](mailto:bkang@udel.edu)  
 † [qzhu8@uncc.edu](mailto:qzhu8@uncc.edu)
- Ahmed Ellaboudy, James L Dye, and Patrick B Smith, "Cesium 18-crown-6 compounds. a crystalline ceside and a crystalline electride," *J. Am. Chem. Soc.* **105**, 6490–6491 (1983).
  - James L. Dye, "Electrons as anions," *Science* **301**, 607–608 (2003).
  - Satoru Matsuishi, Yoshitake Toda, Masashi Miyakawa, Katsuro Hayashi, Toshio Kamiya, Masahiro Hirano, Isao Tanaka, and Hideo Hosono, "High-density electron anions in a nanoporous single crystal:  $[\text{Ca}_{24}\text{Al}_{28}\text{O}_{64}]^{4+}(4e^-)$ ," *Science* **301**, 626–629 (2003).
  - Lee A Burton, Francesco Ricci, Wei Chen, Gian-Marco Rignanese, and Geoffroy Hautier, "High-throughput identification of electrides from all known inorganic materials," *Chem. Mater.* **30**, 7521–7526 (2018).
  - Qiang Zhu, Timofey Frolov, and Kamal Choudhary, "Computational discovery of inorganic electrides from an automated screening," *Matter* **1**, 1293 – 1303 (2019).
  - Xiaoming Zhang, Ruikang Guo, Lei Jin, Xuefang Dai, and Guodong Liu, "Intermetallic  $\text{Ca}_3\text{Pb}$ : a topological zero-dimensional electride material," *J. Mater. Chem. C* **6**, 575–581 (2018).
  - Junjie Wang, Qiang Zhu, Zhenhai Wang, and Hideo Hosono, "Ternary inorganic electrides with mixed bonding," *Phys. Rev. B* **99**, 064104 (2019).
  - Junjie Wang, Kota Hanzawa, Hidenori Hiramatsu, Junghwan Kim, Naoto Umezawa, Koki Iwanaka, Tomofumi Tada, and Hideo Hosono, "Exploration of stable strontium phosphide-based electrides: Theoretical structure prediction and experimental validation," *J. Am. Chem. Soc.* **139**, 15668–15680 (2017).
  - Yaoqing Zhang, Zewen Xiao, Toshio Kamiya, and Hideo Hosono, "Electron confinement in channel spaces for one-dimensional electride," *J. Phys. Chem. Lett.* **6**, 4966–4971 (2015).
  - Yangfan Lu, Jiang Li, Tomofumi Tada, Yoshitake Toda, Shigenori Ueda, Toshiharu Yokoyama, Masaaki Kitano, and Hideo Hosono, "Water durable electride  $\text{Y}_5\text{Si}_3$ : Electronic structure and catalytic activity for ammonia synthesis," *J. Am. Chem. Soc.* **138**, 3970–3973 (2016).
  - Yangfan Lu, Junjie Wang, Jiang Li, Jiazhen Wu, Shu Kanno, Tomofumi Tada, and Hideo Hosono, "Realization of Mott-insulating electrides in dimorphic  $\text{Yb}_5\text{Sb}_3$ ," *Phys. Rev. B* **98**, 125128 (2018).
  - Padtaraporn Chanhom, Kevin E Fritz, Lee A Burton, Jan Kloppeburg, Yaroslav Filinchuk, Anatoliy Senyshyn, Maoyu Wang, Zhenxing Feng, Numpon Insin, Jin Suntivich, et al., "Sr $3\text{Crn}3$ : a new electride with a partially filled d-shell transition metal," *J. Am. Chem. Soc.* **141**, 10595–10598 (2019).
  - Kimoon Lee, Sung Wng Kim, Yoshitake Toda, Satoru Matsuishi, and Hideo Hosono, "Dicalcium nitride as a two-dimensional electride with an anionic electron layer," *Nature* **494**, 336–340 (2013).
  - Tomofumi Tada, Seiji Takemoto, Satoru Matsuishi, and Hideo Hosono, "High-throughput ab initio screening for two-dimensional electride materials," *Inorg. Chem.* **53**, 10347–10358 (2014).
  - Takeshi Inoshita, Sehoon Jeong, Noriaki Hamada, and Hideo Hosono, "Exploration for two-dimensional electrides via database screening and ab initio calculation," *Phys. Rev. X* **4**, 031023 (2014).
  - Daniel L Druffel, Adam H Woome, Kaci L Kuntz, Jacob T Pawlik, and Scott C Warren, "Electrons on the surface of 2d materials: from layered electrides to 2d electrenes," *J. Mater. Chem. C* **5**, 11196–11213 (2017).
  - Biao Wan, Yangfan Lu, Zewen Xiao, Yoshinori Muraba, Junghwan Kim, Dajian Huang, Lailei Wu, Huiyang Gou, Jingwu Zhang, Faming Gao, et al., "Identifying quasi-2D and 1D electrides in yttrium and scandium chlorides via geometrical identification," *npj Computational Materials* **4**, 77 (2018).
  - Tada Tomofumi, Wang Junjie, and Hideo Hosono, "First principles evolutionary search for new electrides along the dimensionality of anionic electrons," *J. Comput. Chem. Jpn* **16**, 135–138 (2017).
  - Sung Wng Kim, Yoshitake Toda, Katsuro Hayashi, Masahiro Hirano, and Hideo Hosono, "Synthesis of a Room Temperature Stable  $12\text{CaO} \cdot 7\text{Al}_2\text{O}_3$  Electride from the Melt and Its Application as an Electron Field Emitter," *Chem. Mater.* **18**, 1938–1944 (2006).
  - Yoshitake Toda, Satoru Matsuishi, Katsuro Hayashi, Kazushige Ueda, Toshio Kamiya, Masahiro Hirano, and Hideo Hosono, "Field emission of electron anions clathrated in subnanometer-sized cages in  $[\text{ca}_{24}\text{al}_{28}\text{o}_{64}]^{4+}(4e^-)$ ," *Adv. Mater.* **16**, 685–689 (2004).

- <sup>21</sup> Jiazhen Wu, Yutong Gong, Takeshi Inoshita, Daniel C Fredrickson, Junjie Wang, Yangfan Lu, Masaaki Kitano, and Hideo Hosono, "Tiered electron anions in multiple voids of lascsi and their applications to ammonia synthesis," *Adv. Mater.* **29**, 1700924 (2017).
- <sup>22</sup> Yoshitake Toda, Hiroshi Yanagi, Eiji Ikenaga, Jung Jin Kim, Masaaki Kobata, Sigenori Ueda, Toshio Kamiya, Masahiro Hirano, Keisuke Kobayashi, and Hideo Hosono, "Work function of a room-temperature, stable electride [ca<sub>24</sub>al<sub>28</sub>o<sub>64</sub>]4+:(e-)4," *Adv. Mater.* **19**, 3564–3569 (2007).
- <sup>23</sup> Masaaki Kitano, Yasunori Inoue, Youhei Yamazaki, Fumitaka Hayashi, Shinji Kanbara, Satoru Matsuishi, Toshiharu Yokoyama, Sung-Wng Kim, Michikazu Hara, and Hideo Hosono, "Ammonia synthesis using a stable electride as an electron donor and reversible hydrogen store," *Nat. Chem.* **4**, 934–940 (2012).
- <sup>24</sup> Masaaki Kitano, Shinji Kanbara, Yasunori Inoue, Navaratnarajah Kuganathan, Peter V Sushko, Toshiharu Yokoyama, Michikazu Hara, and Hideo Hosono, "Electride support boosts nitrogen dissociation over ruthenium catalyst and shifts the bottleneck in ammonia synthesis," *Nature Comm.* **6**, 6731 (2015).
- <sup>25</sup> Junping Hu, Bo Xu, Shengyuan A Yang, Shan Guan, Chuying Ouyang, and Yugui Yao, "2d electrides as promising anode materials for na-ion batteries from first-principles study," *ACS Appl. Mater. Interfaces* **7**, 24016–24022 (2015).
- <sup>26</sup> Tugbey Kocabas, Ayberk Özden, İlker Demiroğlu, Deniz Çakır, and Cem Sevik, "Determination of dynamically stable electrenes toward ultrafast charging battery applications," *J. Phys. Chem. Lett.* **9**, 4267–4274 (2018).
- <sup>27</sup> Jongho Park, Kimoon Lee, Seung Yong Lee, Chandani N Nandadasa, Sungho Kim, Kyu Hyoung Lee, Young Hee Lee, Hideo Hosono, Seong-Gon Kim, and Sung Wng Kim, "Strong localization of anionic electrons at interlayer for electrical and magnetic anisotropy in two-dimensional y<sub>2</sub>c electride," *J. Am. Chem. Soc.* **139**, 615–618 (2017).
- <sup>28</sup> Jongho Park, Jae-Yeol Hwang, Kyu Hyoung Lee, Seong-Gon Kim, Kimoon Lee, and Sung Wng Kim, "Tuning the spin-alignment of interstitial electrons in two-dimensional y<sub>2</sub>c electride via chemical pressure," *J. Am. Chem. Soc.* **139**, 17277–17280 (2017).
- <sup>29</sup> Lauren M McRae, Rebecca C Radomsky, Jacob T Pawlik, Daniel L Druffel, Jack D Sundberg, Matthew G Lanetti, Carrie L Donley, Kelly L White, and Scott C Warren, "Sc<sub>2</sub>c, a 2d semiconducting electride," *J. Am. Chem. Soc.* **144**, 10862–10869 (2022).
- <sup>30</sup> Yunwei Zhang, Weikang Wu, Yanchao Wang, Shengyuan A Yang, and Yanming Ma, "Pressure-stabilized semiconducting electrides in alkaline-earth-metal subnitrides," *J. Am. Chem. Soc.* **139**, 13798–13803 (2017).
- <sup>31</sup> Hu Tang, Biao Wan, Bo Gao, Yoshinori Muraba, Qin Qin, Bingmin Yan, Peng Chen, Qingyang Hu, Dongzhou Zhang, Lailei Wu, et al., "Metal-to-semiconductor transition and electronic dimensionality reduction of ca<sub>2n</sub> electride under pressure," *Adv. Sci.* **5**, 1800666 (2018).
- <sup>32</sup> Gui Wang, Yongle Zhong, Yiguo Xu, Zhengfang Qian, Jingwen Jiang, and Zhuang Ma, "Transition from semiconductor to conductor of a mg<sub>2</sub>n electride induced by strain," *Phys. Chem. Chem. Phys.* **25**, 17300–17305 (2023).
- <sup>33</sup> Gui Wang, Zhuang Ma, Jing-Wen Jiang, Jing-kai Yang, Yi-Ling Sun, Zheng-Fang Qian, Pu Huang, Peng Zhang, and Su-Huai Wei, "Crystal structures and physicochemical properties of be<sub>2</sub>N and mg<sub>2</sub>N as electride materials," *Phys. Rev. Appl.* **19**, 034014 (2023).
- <sup>34</sup> Byungkyun Kang, Kevin Parrish, and Qiang Zhu, "First-principles investigation of electrides derived from sodalites," *J. Phys. Chem. C* **127**, 18745–18754 (2023).
- <sup>35</sup> Anubhav Jain, Shyue Ping Ong, Geoffroy Hautier, Wei Chen, William Davidson Richards, Stephen Dacek, Shreyas Cholia, Dan Gunter, David Skinner, Gerbrand Ceder, et al., "Commentary: The materials project: A materials genome approach to accelerating materials innovation," *Apl Materials* **1**, 011002 (2013).
- <sup>36</sup> Scott Fredericks, Kevin Parrish, Dean Sayre, and Qiang Zhu, "PyXtal: A python library for crystal structure generation and symmetry analysis," *Comput. Phys. Commun.* **261**, 107810 (2021).
- <sup>37</sup> P. E. Blöchl, "Projector augmented-wave method," *Phys. Rev. B* **50**, 17953–17979 (1994).
- <sup>38</sup> G. Kresse and J. Furthmüller, "Efficient iterative schemes for ab initio total-energy calculations using a plane-wave basis set," *Phys. Rev. B* **54**, 11169–11186 (1996).
- <sup>39</sup> John P. Perdew, Kieron Burke, and Matthias Ernzerhof, "Generalized gradient approximation made simple," *Phys. Rev. Lett.* **77**, 3865–3868 (1996).
- <sup>40</sup> Atsushi Togo, Fumiyasu Oba, and Isao Tanaka, "First-principles calculations of the ferroelastic transition between rutile-type and CaCl<sub>2</sub>-type SiO<sub>2</sub> at high pressures," *Phys. Rev. B* **78**, 134106 (2008).
- <sup>41</sup> VI Ponomarev, DM Kheiker, and NV Belov, "Crystal structure of tetracalcium trialuminate-aluminate analog of sodalite," *Soviet Physics Crystallography* **15**, 799 (1971).
- <sup>42</sup> P Smith-Verdier and S Garcia-Blanco, "Redetermination of the structure of anhydrous zinc metaborate zn<sub>4</sub>o (bo<sub>2</sub>)<sub>6</sub>," *Zeitschrift für Kristallographie - Crystalline Materials* **151**, 175–177 (1980).
- <sup>43</sup> Matthew E Brenchley and Mark T Weller, "Synthese, struktur und optische eigenschaften von cd<sub>4</sub>s<sub>6</sub>+clustern in aluminatkäfigen," *Angew. Chem.* **105**, 1726–1727 (1993).
- <sup>44</sup> SE Dann and MT Weller, "Synthesis and structure of cadmium chalcogenide beryllosilicate sodalites," *Inorg. Chem* **35**, 555–558 (1996).
- <sup>45</sup> Axel D Becke and Kenneth E Edgecombe, "A simple measure of electron localization in atomic and molecular systems," *J. Chem. Phys.* **92**, 5397–5403 (1990).
- <sup>46</sup> Leland C Allen, "Electronegativity is the average one-electron energy of the valence-shell electrons in ground-state free atoms," *J. Am. Chem. Soc.* **111**, 9003–9014 (1989).